PHYSICAL REVIEW A, VOLUME 61, 053805

Role of degenerate Zeeman levels in electromagnetically induced transparency

Ying-Cheng Chen, Chung-Wei Lin, and Ite A. Yu
Department of Physics, National Tsing Hua University, Hsinchu, Taiwan 300, Republic of China
(Received 21 April 1999; revised manuscript received 27 July 1999; published 10 April 2000)

We have observed various Λ-type electromagnetically induced transparency (EIT) spectra in laser-cooled ^{87}Rb atoms of different laser polarization configurations. Unexpected profiles occur in the EIT spectra. We have found the degenerate Zeeman sublevels are responsible for these profiles. The experimental data are in good agreement with the results from the theoretical calculation which takes into account all the 13 Zeeman levels in the Λ system. Our study demonstrates that Zeeman sublevels play important roles in quantum interference phenomena such as EIT and amplification without population inversion (AWI), and should be taken into account in the analysis of these phenomena.

PACS number(s): 42.50.Gy, 42.62.Fi, 32.80.Pj

Since the phenomenon of electromagnetically induced transparency (EIT) [1] was first proposed and observed [2,3], it has attracted great attention along with its applications and the related effects such as lasing without population inversion (LWI) [4], coherence population trapping (CPT) [5], enhancement of nonlinear wave mixing [6,7], and modification of the refractive index [8,9]. Recently, it gains more popularity to employ laser-cooled atoms in studying these quantum interference phenomena [10–14,17–19]. The effect of Doppler broadening is eliminated in cold atoms with temperatures below mK. This allows the coupling and the probe beams to propagate in arbitrary directions and to have various kinds of polarization configurations in the experiments of studying these phenomena. The flexibility of the experimental arrangements and the degree of freedom of the studies are improved. In addition, the motion of cold atoms is very slow. One can have very high density sample of cold atoms for the studies and the collision perturbation is still negligible. This can greatly enhance the quantum interference effects. We therefore choose to use laser-cooled ^{87}Rb atoms to study the Λ-type EIT.

In this work, an unexpected profile appears in the EIT spectrum which, in our knowledge, has not been demonstrated in the literature. This has prompted the motivation of the study. We vary the polarization configurations of the laser fields and obtain different EIT spectra. The result indicates that the degenerate Zeeman sublevels play important roles in the EIT spectra. In order to clarify the experimental data, we conduct the theoretical calculation that considers all the Zeeman levels. The results of the theoretical calculation are in good agreement with the experimental data. We provide a simple theoretical picture to explain the observed spectra. Our final step is to extend the theoretical calculation to predict spectra of room-temperature samples.

Figure 1 illustrates the experimental arrangement. Cold ^{87}Rb atoms are produced with a vapor-cell magneto-optical trap (MOT) [15,16]. Pressure of the vapor cell is about 4×10^{-9} Torr. The MOT is formed with a spherical quadrupole magnetic field, six trapping laser beams, and a repumping laser beam. Two anti-Helmholtz coils generate the spherical quadrupole magnetic field with an axial gradient of 12 G/cm. The circular trapping beams have $1/e$ diameters of 9.6 mm and the power of each trapping beam is 2.3 mW. Its frequency is tuned to 15 MHz below the $5S_{1/2},F=2\rightarrow5P_{3/2},F'=3$ transition. The repumping beam drives the $5S_{1/2},F=1\rightarrow5P_{3/2},F'=2$ transition with an $1/e$ diameter of 10 mm and a power of 4 mW. Typically, we trap 5×10^{7} atoms with a temperature of 400 μK in the MOT. We use a coupling laser beam and a weak probe laser beam to measure EIT spectra. The frequency of the coupling laser is locked to the $5S_{1/2},F=1\rightarrow5P_{3/2},F'=2$ transition, while

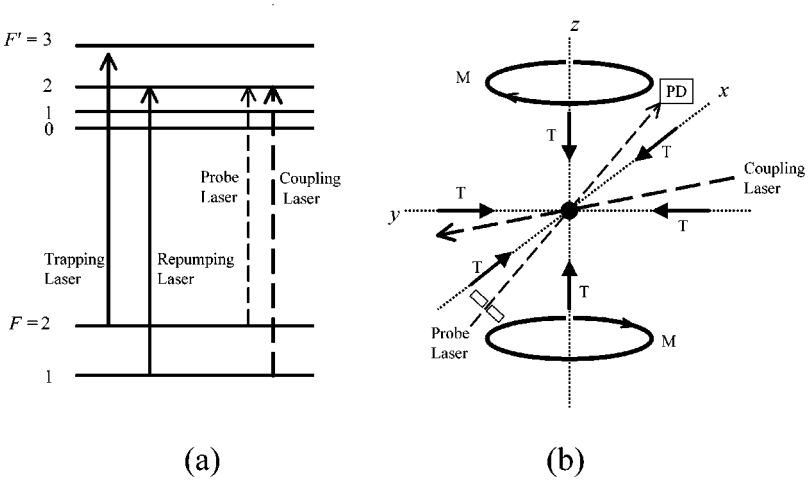

FIG. 1. (a) The diagram of ^{87}Rb energy levels. (b) The scheme of the experiment. T denotes the trapping beams and **M** denotes the anti-Helmholtz coils. The repumping beam is not shown in the figure. The coupling and probe beams propagate in the xy plane and their propagation directions are orthogonal. **PD** is the photodetector for measuring the probe absorption.

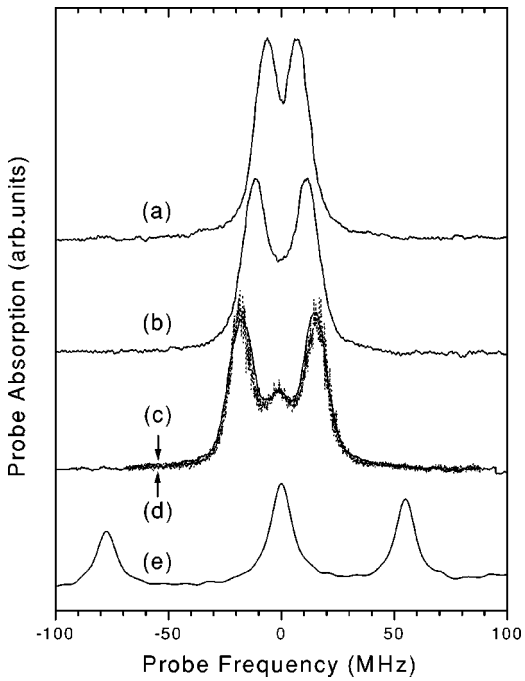

FIG. 2. (a), (b), (c), and (d) are the probe absorption spectra of cold ^{87}Rb atoms. The averaged intensities of the coupling beam in the atom cloud are 100, 220, and 420 mW/cm^2 for (a), (b), and (c) and (d), respectively. (e) is the saturated absorption spectrum of a room-temperature Rb vapor.

that of the probe laser is scanned across the $5S_{1/2},F=2 \rightarrow 5P_{3/2},F'=2$ transition. Both lasers have linewidths less than or equal to 1 MHz. The coupling beam is in elliptical shape with major and minor $1/e$ diameters of 3.4 and 1.7 mm. Cold atoms produced by the MOT are completely inside this $1/e$ beam profile of the coupling laser. The profile of probe beam is also elliptical with major and minor $1/e$ diameters of 1.1 and 0.6 mm. Before the probe beam interacts with the atoms, it is sent through a circular aperture with a diameter of 0.6 mm. We keep the power of the circular probe beam at 1.5 μW through the entire measurements. The coupling and probe beams propagate in the orthogonal directions which are denoted as $\hat{y}'$ and $\hat{x}'$, respectively. In this experiment, the trapping, repumping, coupling, and probe beams come from four independent diode lasers.

Curves (a), (b), and (c) in Fig. 2 show the EIT spectra of the cold ^{87}Rb atoms for different coupling beam intensities in the presence of the MOT. The coupling beam is linearly polarized in the direction of $\hat{x}'$ and the probe beam is linearly polarized in the direction of $\hat{z}$. We determine the probe laser frequency with the saturated absorption spectrum of a room-temperature Rb vapor as shown in curve (e). The mark of 0 in the horizontal scale in Fig. 2 indicates the resonance frequency of the $F=2 \rightarrow F'=2$ transition. When the intensity of the coupling beam increases, the dip around the center of the $F=2 \rightarrow F'=2$ transition in the probe absorption spectrum gets wider and deeper as expected. However, curve (c) in Fig. 2 differs from all the other EIT spectra that we have seen in the literature, e.g., Refs. [12–14,17–20]. An unexpected bump emerges inside the dip of that curve. This unexpected spectrum is independent of the absolute orientation of the laser polarization in the space. We keep the polarization direction of the coupling beam in the $\hat{x}'$ and rotate that of the probe beam to any direction perpendicular to $\hat{x}'$. We also try the polarization direction of the probe beam in $\hat{y}'$ and rotate that of the coupling beam to any direction perpendicular to $\hat{y}'$. The observed spectra in any of the above situations are the same as the one shown in curve (c). The unexpected bump is also not caused by the presence of the MOT. We perform the measurements of the probe absorption spectra when the MOT is temporarily shut off (an 1-ms interval) and all the other conditions are kept the same as those of curve (c). The signals of such measurements are smaller and much noisier. Curve (d) is the average of 5 times of such measurements and normalized to the height of curve (c). Due to the laser-field excitations and the magnetic-field inhomogeneity of the MOT, the spectral width in curve (c) is a little broader than that in curve (d). Except for this difference, curve (d) is in agreement with curve (c). Although the presence of the MOT can perturb the measured spectra, the perturbations do not influence our study much due to the reasons below. The frequency of the trapping beams is far from the resonance of the studied transition; all the light shifts of the $5S_{1/2},F=2$ Zeeman states induced by the trapping field are much smaller than the Rabi frequency of the coupling field; the average amount of these light shifts is estimated to be 1.5 MHz and such amount is less than the uncertainty ($\approx \pm 3$ MHz) of our frequency determination; the intensity of the repumping beam is much weaker than that of the coupling beam; the Zeeman shift caused by the magnetic field in the region of the atom cloud is much smaller than the Rabi frequency of the coupling field; the broadening of the spectra due to the fields of the MOT does not modify the spectral feature of our study. The rest of our experimental study is under the presence of the MOT for better signal to noise ratio.

In Fig. 3, we vary the polarization configurations of the coupling and probe beams. The vertical scale of the normalized probe absorption in the figure is chosen such that the peak absorption of the probe beam is 1 in the absence of the coupling beam. The probe frequency is also determined in the same way as shown in Fig. 2. The mark of 0 in the horizontal scale in Fig. 3 indicates the resonance frequency of the $F=2 \rightarrow F'=2$ transition. The various polarization configurations of the coupling and probe beams result in quite different spectra. These experimental data reveal that the degenerate Zeeman levels play important roles in the EIT spectra.

In order to clarify the above experimental results, we perform the theoretical calculation of the probe absorption spectrum that considers all the 13 Zeeman levels in the Λ system [21,26]. Our calculations are limited to the cases that the coupling field is linearly polarized and the magnetic field is absent. Two examples of the excitations of the coupling and the probe beams are illustrated in Fig. 4. Figure 4(a) shows that the directions of the linear polarizations of the two beams are parallel and (b) corresponds orthogonal. For the excitations in Fig. 4(a), the density matrix ρ is solved with the following equations:

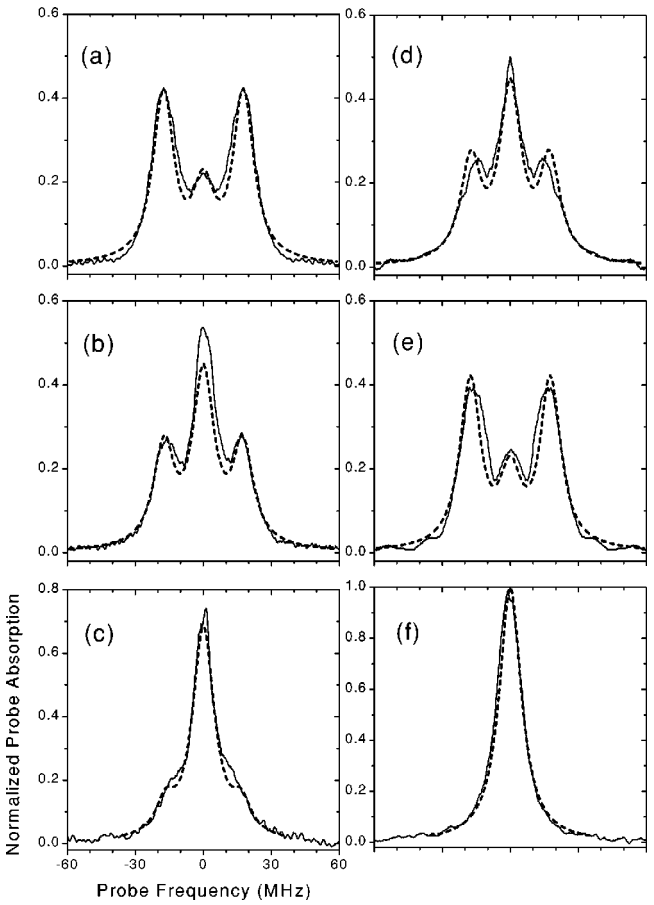

FIG. 3. The average intensity of the coupling beam is 420 mW/cm^2. The solid and dashed lines are the experimental and theoretical spectra, respectively. The coupling and probe beams are polarized in (a) $\hat{z}$ and $\hat{y}'$, (b) $\hat{z}$ and $\hat{z}+\hat{y}'$, (c) $\hat{z}$ and $\hat{z}$, (d) $\hat{z}$ and σ_+ (σ_-), and (e) $\hat{x}'$ and σ_+ (σ_-). In (d) and (e), the spectra of the σ_+ and σ_- polarizations of the probe beam are the same. (f) The coupling beam is off. We use $\Gamma'=0.5\Gamma$ and $\Gamma''=0.7\Gamma$ in the theoretical calculation.

$$\frac{d\rho}{dt}=\frac{1}{i\hbar}[H_{\rm atom}+H_{\rm coupling}+H_{\rm probe},\rho]+\left\{\frac{d\rho}{dt}\right\}, \tag{1}$$

$$H_{\rm atom}=\hbar\omega_{21}\sum_{i=9}^{13}|i\rangle\langle i|+\hbar(\omega_{21}-\omega_{22})\sum_{i=4}^{8}|i\rangle\langle i|, \tag{2}$$

$$H_{\rm coupling}=-e^{i\omega_c t}\left[\frac{\hbar\Omega_{c1}}{2}(|1\rangle\langle 10|+|3\rangle\langle 12|)+\frac{\hbar\Omega_{c2}}{2}|2\rangle\langle 11|\right]+\text{c.c.}, \tag{3}$$

$$H_{\rm probe}=-e^{i\omega_p t}\left[\frac{\hbar\Omega_{p1}}{2}(|4\rangle\langle 9|+|8\rangle\langle 13|)+\frac{\hbar\Omega_{p2}}{2}(|5\rangle\langle 10|+|7\rangle\langle 12|)\right]+\text{c.c.}, \tag{4}$$

$$\begin{aligned}\left\{\frac{d\rho}{dt}\right\}=&-\Gamma\sum_{i=9}^{13}\rho_{ii}|i\rangle\langle i|+\sum_{i=1}^{8}\left(\sum_{j=9}^{13}\Gamma_{ji}\rho_{jj}\right)|i\rangle\langle i|\\&-\frac{\Gamma}{2}\left[\sum_{i=9}^{13}\sum_{j=1}^{8}\rho_{ij}|i\rangle\langle j|+\text{c.c.}\right]\\&-\Gamma'\left[\sum_{i=9}^{13}\sum_{j=1}^{8}\rho_{ij}|i\rangle\langle j|+\text{c.c.}\right]\\&-\Gamma''\left[\sum_{i=1}^{3}\sum_{j=4}^{8}\rho_{ij}|i\rangle\langle j|+\text{c.c.}\right].\end{aligned} \tag{5}$$

In the equation of $H_{\rm atom}$, ω_{21} is the $F=1\rightarrow F'=2$ transition frequency and ω_{22} is the $F=2\rightarrow F'=2$ transition frequency. The equations of $H_{\rm coupling}$ and $H_{\rm probe}$ are written in the rotating wave approximation. ω_c is the frequency of the coupling laser and ω_p is that of the probe laser. Ωs are the Rabi frequencies and their subscripts indicate the different transitions. The equation of $\{d\rho/dt\}$ describes all the relaxation processes in the system. $\Gamma=2\pi\times 5.9$ MHz is the spontaneous decay rate of the $5P_{3/2}$,$F'=2$ excited state. Γ_{ji} is the spontaneous emission rate from an excite state $|j\rangle$ to a ground state $|i\rangle$. Γ' and Γ'' are the decoherence rates for the relaxation processes other than the spontaneous decay. The linewidths (γ_l) of the laser fields and the magnetic-field inhomogeneity (γ_m) in the experiment contribute Γ' ($\approx\gamma_l+\gamma_m$) and Γ'' ($\approx 2\gamma_l+\gamma_m$) mostly. Treating the weak $H_{\rm probe}$ as the perturbation, the calculation is carried out to all orders of $H_{\rm coupling}$ and to the first order of $H_{\rm probe}$ [22]. After the stationary solution of Eq. (1) is found, the probe absorption cross section is the imaginary part of

$$\frac{3\lambda^2}{2\pi}e^{i\omega_p t}\sum_{i,j}\Gamma_{ij}\langle F'=2,m_z=i|\rho|F=2,m_z=j\rangle/\Omega_{ij}. \tag{6}$$

In the above, the summation is for all the allowed probe transitions, λ is the wavelength of the probe beam, Γ_{ij} is the spontaneous emission rate from $F'=2,m_z=i$ to $F=2,m_z=j$, and Ω_{ij} is the Rabi frequency of the $F=2,m_z=j$ to $F'=2,m_z=i$ transition. For the excitations in Fig. 4(b), the probe Hamiltonian is changed to

$$\begin{aligned}H_{\rm probe}=-e^{i\omega_p t}\Bigg[&\frac{\hbar\Omega'_{p1}}{2}(|4\rangle\langle 10|+|8\rangle\langle 12|)\\&+\frac{\hbar\Omega'_{p2}}{2}(|5\rangle\langle 9|+|7\rangle\langle 13|)\\&+\frac{\hbar\Omega'_{p3}}{2}(|5\rangle\langle 11|+|7\rangle\langle 11|)\\&+\frac{\hbar\Omega'_{p4}}{2}(|6\rangle\langle 10|+|6\rangle\langle 12|)\Bigg]+\text{c.c.}\end{aligned} \tag{7}$$

and the remaining part of the calculation is similar. All the theoretical spectra of the different polarization configurations are obtained in the same way.

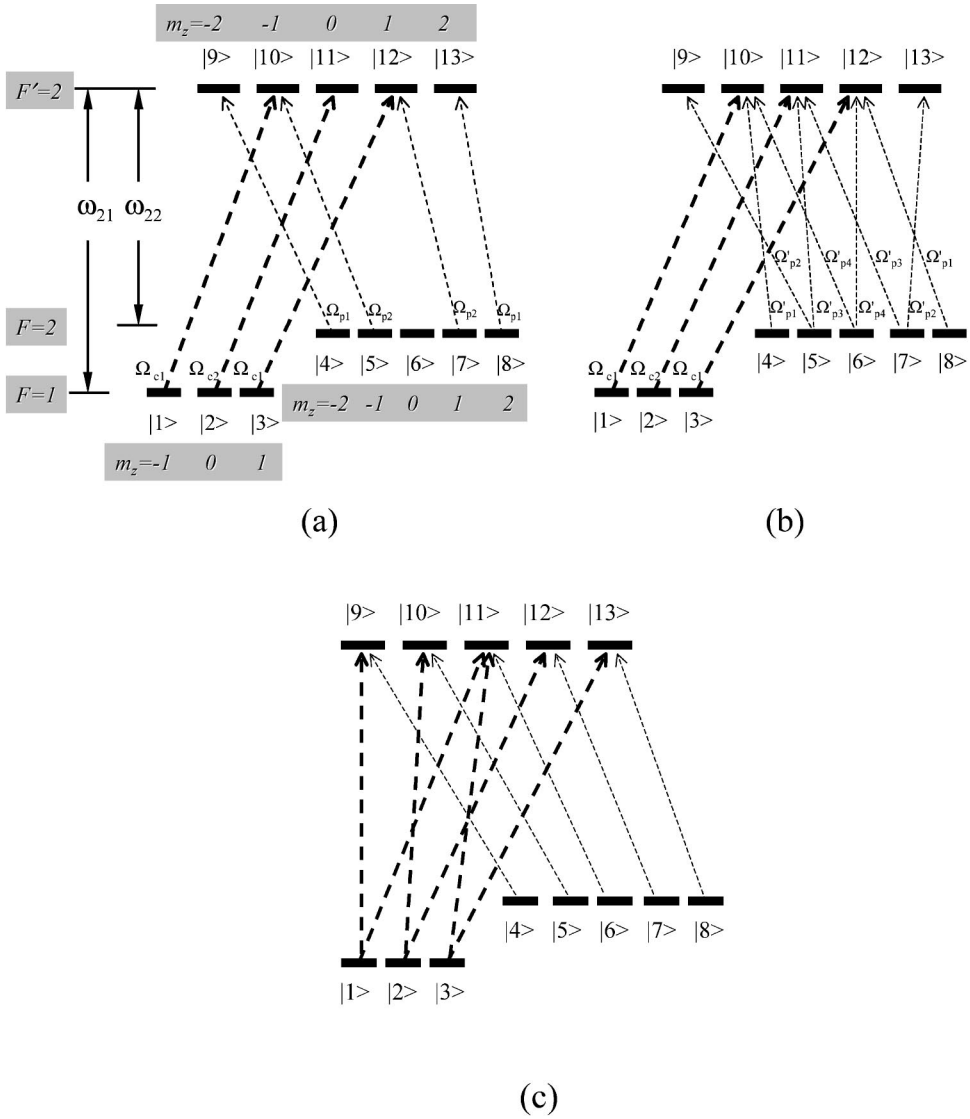

FIG. 4. The excitations of the coupling and probe fields among the Zeeman levels in the Λ system. The coupling and probe beams are linearly polarized. Their polarization directions are parallel in (a) and orthogonal in (b). The probe transition of $|6\rangle \rightarrow |11\rangle$ in (a) is forbidden. The polarization configurations of (a) and (b) result in the spectra of Figs. 3(c) and 3(a), respectively.

The results of the theoretical calculation are in good agreement with the experimental data as demonstrated in Fig. 3. We also compare the experimental and theoretical spectra of the probe absorption around the $F=2 \rightarrow F'=1$ transition, when the frequency of the coupling laser is locked to the $F=1 \rightarrow F'=1$ transition frequency. The observed probe spectra in such arrangement are similar to those in Fig. 3. There are bumps or peaks around the resonance frequency in the observed probe spectra. For the different polarization configurations of the coupling and probe beams, the consistency between the experimental and theoretical spectra is satisfactory.

When we consider all the degenerate Zeeman sublevels in the Λ system, the reason of the unexpected profiles of the EIT spectra becomes clear. For example, Fig. 4(b) shows $|5\rangle \rightarrow |9\rangle$ and $|7\rangle \rightarrow |13\rangle$ of the probe transitions without the interference of the coupling field. Such probe transitions (nondark transitions) result in a Lorentzian profile with a peak at the resonance frequency. All the probe transitions (dark transitions) other than $|5\rangle \rightarrow |9\rangle$ and $|7\rangle \rightarrow |13\rangle$ result in an EIT profile. The observed spectrum is the combination of the Lorentzian profile and the EIT profile. In the case of Fig. 4(b), the intensity of the Lorentzian profile is much smaller than that of the EIT profile. The peak of the Lorentzian profile protrudes in the dip of the EIT profile such as a small bump as shown in Fig. 2(c) or Fig. 3(a). When the coupling beam is not strong and the EIT dip is not too deep and wide, the small Lorentzian profile is concealed and becomes unnoticeable as shown in Figs. 2(a) and 2(b). On the other hand, the intensity of the Lorentzian profile is comparable to that of the EIT spectrum in the case of Fig. 4(a). A narrower Lorentzian shape can be seen clearly on the top of the broader EIT profile as shown in Fig. 3(c). Although our experimental observations were carried out in the regime of high coupling field intensity where the spectra of the dark transitions can be seen as Autler-Townes doublets [13,18],

the above illustration about the bump is still valid. At low coupling field intensity where the spectra of the dark transitions are undoubted EIT phenomena, one can also expect that the nondark transitions will degrade the EIT effect.

We also examine the other two Λ-type EIT systems in the $5S_{1/2}$ and the $5P_{3/2}$ states of ^{87}Rb atoms, while the coupling field is linearly polarized. In one case, the probe field drives $F=1\rightarrow F'=2$ transitions and the coupling field drives $F=2\rightarrow F'=2$ transitions. Because the $F=2,m_F=0\rightarrow F'=2,m_F'=0$ transition is forbidden, the nondark transition of the probe will still exist in all kinds of polarization configurations. In the case that the probe field drives $F=1\rightarrow F'=1$ transitions and the coupling field drives $F=2\rightarrow F'=1$ transitions, all probe transitions will be dark transitions in all polarization configurations. In the Λ-type EIT systems of the $5S_{1/2}$ and $5P_{3/2}$ states of ^{87}Rb atoms with a linearly polarized coupling field, this is the only arrangement of the laser frequencies that will not have any nondark transition.

We further extend the theoretical calculation to a room-temperature sample [23]. The calculation considers all the 13 Zeeman levels, and assume that the coupling and probe beams are copropagating to eliminate the Doppler effect. The two solid curves predicted from the 13-level calculation in Fig. 5 are the spectra of the orthogonal and parallel polarization configurations of the coupling and probe beams. The absorption-reduction dips of the two spectra differ greatly in depth. This indicates that proper arrangement of a laser-polarization configuration or proper selection of hyperfine levels will certainly improve the absorption reduction or the amplification gain in EIT or LWI experiments with room-temperature samples. The dashed curve in Fig. 5 is the predicted spectra of the orthogonal polarization configuration from a three-level calculation. The three-level calculation does not consider the degenerate Zeeman sublevels and uses the average Rabi frequency of all the coupling transitions. The spectra of the orthogonal polarization configuration from the 13-level and three-level calculations differ a little. Although the three-level calculation cannot deal with laser polarization, it can be fair to predict spectra of a room-temperature sample in the orthogonal laser-polarization configuration.

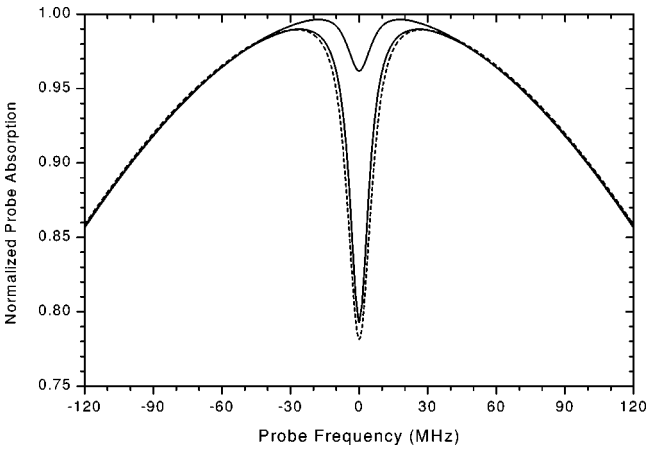

FIG. 5. The EIT spectra of room-temperature ^{87}Rb atoms for the excitations described in Figs. 4(a) and 4(b). The vertical scale is chosen such that the peak absorption of the probe beam is 1 in the absence of the coupling beam. The top spectrum is in the parallel polarization configuration. The lower two spectra are in the orthogonal polarization configuration. The spectra from the 13-level calculation are shown in the solid lines and the spectrum from the three-level calculation is shown in the dashed line. The intensity of the coupling beam is 420 mW/cm^2. $\Gamma'=0.5\Gamma$ and $\Gamma''=0.7\Gamma$.

In summary, we have demonstrated experimentally and theoretically that the degenerate Zeeman levels play important roles in the EIT spectra. Only the calculation that takes into account all the degenerate Zeeman levels can predict spectra properly for different laser-polarization configurations. The experimental data are in good agreement with the results of the theoretical calculation. Our study shows that Zeeman sublevels should be taken into account in the analysis of the quantum interference effects such as EIT and AWI. Other than our demonstration, the effect and the importance of Zeeman sublevels in cold atom spectroscopy or in quantum interference phenomena have also been presented in Refs. [24–27].

This work is supported by the National Science Council of the Republic of China under NSC Grant No. 88-2112-M-007-047. We thank Professor Jow-Tsong Shy and Dr. Mao-Sheng Huang for loaning us some instruments.

[1] For a recent review, see J. P. Marangos, J. Mod. Opt. **45**, 471 (1998).
[2] A. Imamoğlu and S. E. Harris, Opt. Lett. **14**, 1344 (1989).
[3] K. J. Boller, A. Imamoğlu, and S. E. Harris, Phys. Rev. Lett. **66**, 2539 (1991).
[4] G. G. Padmabandu, G. R. Welch, I. N. Shubin, E. S. Fry, D. E. Nikonov, M. D. Lukin, and M. O. Scully, Phys. Rev. Lett. **76**, 2053 (1996).
[5] For a recent review, see E. Arimondo, in *Progress in Optics XXXV*, edited by A. Wolf (Elsevier, Amsterdam, 1996), p. 258.
[6] S. E. Harris, J. E. Field, and A. Imamoğlu, Phys. Rev. Lett. **64**, 1107 (1990).
[7] Y. Q. Li and M. Xiao, Opt. Lett. **21**, 1064 (1996).
[8] S. E. Harris, J. E. Field, and A. Kasapi, Phys. Rev. A **46**, 29 (1992).
[9] M. Xiao, Y. Q. Li, S. Jin, and J. Gea-Banacloche, Phys. Rev. Lett. **74**, 666 (1995).
[10] L. V. Hau, S. E. Harris, Z. Dutton, and C. H. Behroozi, Nature (London) **397**, 594 (1999).
[11] J. Kitching and L. Hollberg, Phys. Rev. A **59**, 4685 (1999).
[12] M. Mitsunaga and N. Imoto, Phys. Rev. A **59**, 4773 (1999).
[13] T. van der Veldt, J.-F. Roch, P. Grelu, and P. Grangier, Opt. Commun. **137**, 420 (1997).
[14] F. S. Cataliotti, C. Fort, T. W. Hänsch, M. Inguscio, and M. Prevedelli, Phys. Rev. A **56**, 2221 (1997).
[15] E. L. Raab, M. Prentiss, A. Cable, S. Chu, and D. E. Pritchard, Phys. Rev. Lett. **59**, 2631 (1987).
[16] C. Monroe, W. Swann, H. Robinson, and C. Wieman, Phys.

Rev. Lett. **65**, 1571 (1990).
[17] H. X. Chen, A. V. Durrant, J. P. Marangos, and J. A. Vaccaro, Phys. Rev. A **58**, 1545 (1998).
[18] S. A. Hopkins, E. Usadi, H. X. Chen, and A. V. Durrant, Opt. Commun. **138**, 185 (1997).
[19] A. V. Durrant, H. X. Chen, S. A. Hopkins, and J. A. Vaccaro, Opt. Commun. **151**, 136 (1998).
[20] M. Mitsunaga, T. Mukai, K. Watanabe, and T. Mukai, J. Opt. Soc. Am. B **13**, 2696 (1996).
[21] H. Y. Ling, Y. Q. Li, and M. Xiao, Phys. Rev. A **53**, 1014 (1996).
[22] G. Grynberg, M. Pinard, and P. Mandel, Phys. Rev. A **54**, 776 (1996).
[23] J. Gea-Banacloche, Y. Q. Li, S. Jin, and M. Xiao, Phys. Rev. A **51**, 576 (1995).
[24] D. Grison, B. Lounis, C. Salomon, J. Y. Courtois, and G. Grynberg, Europhys. Lett. **15**, 149 (1991).
[25] A. M. Akulshin, S. Barreiro, and A. Lezama, Phys. Rev. A **57**, 2996 (1998).
[26] A. Lezama, S. Barreiro, and A. M. Akulshin, Phys. Rev. A **59**, 4732 (1998).
[27] A. M. Akulshin, S. Barreiro, and A. Lezama, Phys. Rev. Lett. **83**, 4277 (1999).